A Comparison of the Passive Oxide Films Formed on CANDU Steam Generator Tubing Alloy 600 and Alloy 800.

M. Faichuk[1], S. Ramamurthy,[2]Jamie Noël[1], W. M. Lau[*], D.W. Shoesmith[1,2]
[1] University of Western Ontario, Department of Chemistry, Ontario, Canada
[2] Surface Science Western, Ontario, Canada

Abstract

Alloy 600 (A600) steam generator (SG) tubing has been shown to be susceptible to stress corrosion cracking (SCC). Alloy 800 (A800) was developed as a replacement, though it has shown susceptibility to corrosion under certain conditions. The properties of the passive oxide films on both alloys were extensively analyzed to determine why the performance of A800 is superior to that of A600. Surface analysis to determine oxide composition was performed using X-ray photoelectron spectroscopy (XPS) and Auger Electron spectroscopy (AES). Electrochemical measurements were made using anodic polarization and electrochemical impedance spectroscopy (EIS). The oxide films on A600 and A800 were shown to have different electrochemical and compositional properties.

1. Introduction

New materials are currently being studied for use in nuclear power stations as steam generator (SG) tubing. Alloy 600 (A600) used to be one of the “superalloys” for this application but numerous reports over the years have detailed the underlying issues with the A600 tubing, and the problem with its susceptibility to stress corrosion cracking (SCC) (1,2).The SG tubing is often subjected to harsh operating conditions, such as high pressures and temperatures. SCC is the result of exposing a susceptible material exposed simultaneously to a corrosive environment and residual or applied stress. This type of corrosion can be very severe, as catastrophic damage can occur even though the stress levels are within the specified range for normal operating conditions (3). In the industrial setting, SCC of SG tubing can result in highly radioactive primary water leaking out and mixing with the secondary water. This creates enormous safety and financial problems, as the whole plant must be shut down in order to repair the tubing.

A possible replacement for this material is Alloy 800 (A800), which was designed to be much more resistant to corrosion at higher temperatures (4, 5, 6). This type of tubing is already being used in reactors in Canada, Germany, and other countries. Literature has shown that, while A600 is much more susceptible to SCC, A800 itself is not totally immune. Recent reports have shown that under more extreme operating conditions, A800 has experienced SCC (7). SCC also becomes an issue when higher temperatures and pressures are used to maximize the efficiency of the CANDU™ reactors.

Since SCC is highly dependent upon the properties of the passive oxide formed on the alloy, a better understanding of this film is required. Many studies on the various types of corrosion observed on A800have been reported in the literature, but there are few publications that deal with surface analysis. There are even fewer studies that can correlate the electrochemical behaviour of the alloy with the composition of the passive film. Recently, a study of A600 in a thiosulphate solution, looking at how the changes in the passive film could affect the electrochemical behaviour of the alloy, was published (8). Electrochemical methods such as electrochemical impedance spectroscopy (EIS) were used to understand the corrosion behaviour, while surface analytical tools like X-ray photoelectron spectroscopy (XPS) and Auger electron spectroscopy (AES) were used to quantify the film composition. Using thiosulphate, which has been known to destabilize the oxide film, the formation and breakdown of the passive film were observed and analysed from two different perspectives (7).The overall objective of the current study is to compare the electrochemical behaviours of both A600 and A800 in a thiosulphate solution and correlate these changes to differences in oxide composition. This could lead to a better understanding of each element's role in the passivation of the film at different potentials.

2. Experimental

9.5 mm diameter A 600 and A800 tubing sections were procured from Rolled Alloys Canada in the mill-annealed condition. The composition of these alloys is presented in Table 1. Small rectangular prismatic coupons were cut from this tubing using a BuehlerJ diamond-tipped saw. The average area on the outer surface of these coupons was 20 mm^2. The coupons were polished, finishing with a 0.05 μm alumina grit polishing pad and washed with deionized water and sonicated in acetone. Bulk compositional differences between the two alloys are shown in Table 1. The most significant changes occurred for elements Ni, Cr and Fe.

	Ni	**Cr**	**Fe**	**Mn**	**Al**	**Ti**	**Si**	**C**	**S**
A600	73.19	16.14	9.65	0.34	0.27	0.23	0.15	0.03	0.001
A800	30.86	20.37	46.49	0.72	0.40	0.53	0.54	0.07	0.012

Table 1 Bulk elemental composition (wt.%) of Alloy 600 and 800.

Electrochemical measurements were carried out using the sample coupons. Electrodes were assembled by spot welding a stainless steel wire onto the polished coupon. The back and sides of the coupon, as well as the wire, were coated with a microshield™ masking aid. A de-areated solutionof 0.1 M $Na_2S_2O_3$at room temperature was used for the electrochemical experiments. The three-electrode cell consisted of a platinum foil counter electrode, a saturated calomel reference electrode (0.2412 V vs SHE), and the A600 and A800 coupons acting as the working electrode. At the beginning of each experiment, a reducing potential of -1.2 V_{SCE} was applied for 30 seconds. Potentiodynamic polarization experiments were run using a Solartron 1286 potentiostat (scan rate 0.167 mV/s). The experiments were started 0.150 V_{SCE} below the measured open circuit potential and were terminated at 1 V_{SCE}.

Using the same preparation technique, electrochemical analysis of the samples was conducted using EIS.The cell set-up remained unchanged, and pre-treatment measures included cathodic cleaning at -1.2 V_{SCE}, followed by exposure to an applied potential for 8 hours. Potentials selected for analysis were determined based on the anodic polarization curve.The frequency range was between 65 kHz to

0.01 Hz, with measurements made using a Solartron 1250 frequency response analyzer. The data was collected and modeled using ZPlot™ and ZView™ software, respectively.

Auger data was obtained using a PHI 660 Auger electron spectrometer with an excitation energy of 5 keV. An Ar^+ ion beam was used for sputtering to obtain depth profile measurements. In order to ensure proper conductivity, the masking agent was stripped from the sample and the wire, which had been previously spot wielded onto the sample, was removed in order to fit into the coupon into the sample holder. For each sample, a survey scan was acquired, and during depth profiling the intensity for elements such as Ni, Cr, Fe, C, and O was monitoredas a function of sputter time. For each sample, two separate spots were analyzed, and when it was determined that the results were reproducible, an average of these values was calculated and used in the data analysis.

XPS analyses were conducted on the sample electrodes after electrochemical growth of the oxide film. Immediately following treatment, samples were rinsed with DI water and methanol. A Kratos AXIS Ultra spectrometer was employed for analysis using a monochromatic Al Kα electron source (15 mA, 14 kV). For each sample, survey scan analyses were carried out over an area of 256 x 256 μm at a pass energy of 160 eV between 0 to 1000 eV. High resolution scans of Ni $2p_{3/2}$, Cr $2p_{3/2}$, C 1s and O 1s peaks were obtained at a pass energy of 20 eV from the same area with a step size of 0.05 eV. Spectral analysis was performed using CasaXPS™ software. With the exception of Cr $2p_{3/2}$, all spectra have been charge corrected to the main line of the C 1s spectrum. Both high resolution and survey scans were collected on two different spots in the sample surface to ensure reproducibility. The reported data is an average of these two spots.

3. Results and Discussion

3.1 Electrochemical Results

Figure 1 shows the anodic polarization curves of both A600 and A800 that were run in a 0.1 M $Na_2S_2O_3$ solution. The results show that both curves possess many similar features throughout the measured potential range. The passive region spanned a range of -0.4 V_{SCE} to 0.75 V_{SCE}. This range was then divided into two regions based on the change in slope at 0.2 V_{SCE}, passive region I (-0.4 V_{SCE} to 0.2 V_{SCE}) and passive region II (0.2 V_{SCE} to 0.75V_{SCE}). An anodic peak observed at 0.1V_{SCE} for both alloys. One major difference between the two curves is that the current density measured for A800 is nearly an order of magnitude lower than that of A600, suggesting reduced reactivity on the surface.

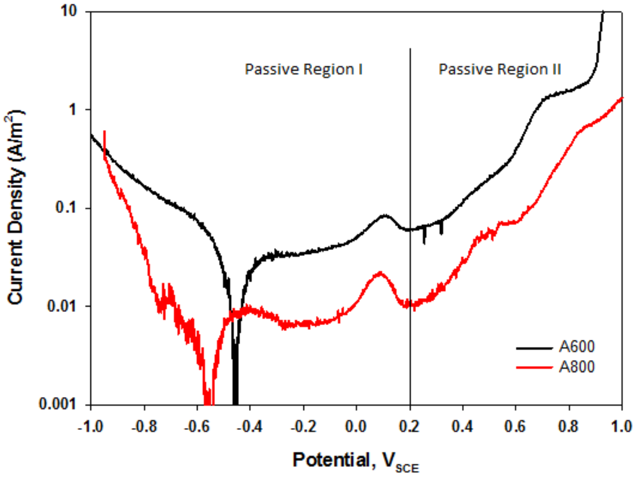

Figure 1 Anodic polarization curves of A600 and A800 in 0.1 M $Na_2S_2O_3$ solution.

Electrochemical impedance measurements were carried out at various potentials within the entire passive region for both alloys. An equivalent circuit containing two time constants in series was used to fit the impedance data, which is typical for the bilayer oxide film in this system. According to the resistance values of both layers obtained from the model, the inner barrier layer provided significantly more protection against corrosion than did the outer layer, within the passive region.

3.2 Surface Analysis

Surface analysis was performed on the samples after the oxide film was electrochemically grown at various potentials, and this data was correlated to changes in electrochemical behaviour. Using the data collected from Auger depth profiling, it was found that the bilayer oxide film on both alloys contained a Cr-rich barrier layer, and an outer layer rich in Ni and/or Fe. The applied potential had a significant effect on the film composition, especially between the two passive regions. An interesting finding from the AES data revealed that the structure of the bilayer film varied between the two alloys. On A800, two separate, distinct layers were observed; the majority of the Cr was concentrated into the barrier (inner) layer, while most of the Fe or Ni was located within the outer layer. A600, on the other hand, appeared to contain two layers, but the division between the inner and outer layer was not as distinct as it was for A800. The composition of the passive films also varied between the two alloys, especially within the outer layer. A800 contained much more Fe, while A600 had more Ni in the outer layer.

Using the results obtained from the XPS analysis, a schematic diagram was drawn up for both alloys. Figure 2 shows the changes in the oxide film between the two passive regions.

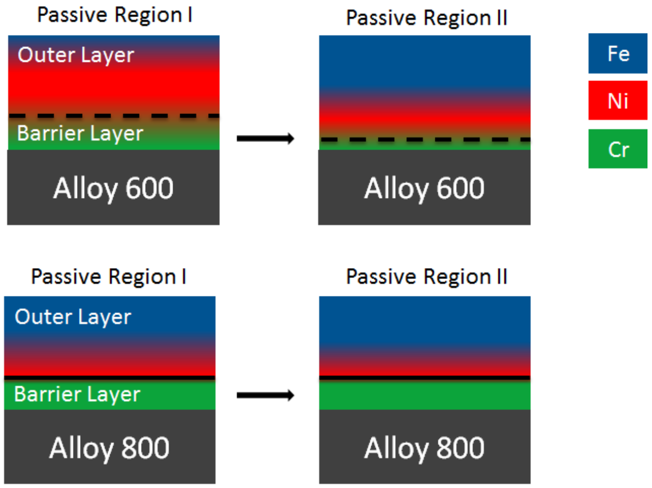

Figure 2 Schematic diagram of the passive bilayer oxide film on Alloy 600 and 800 at two different potential ranges.

For both alloys, the barrier layer contained a high concentration of Cr_2O_3 (green), and the outer layer contained a mixture of $Ni(OH)_2$ (red) and Fe oxides (blue). Between passive regions I and II, A600 experiences a breakdown of the barrier layer, and a significant portion of Cr is lost. There is also a loss of $Ni(OH)_2$, and the subsequent accumulation of Fe oxides. A800, however, appears to retain the barrier layer at the higher potentials which could be a reason for the increase in corrosion resistance. Only minor changes in Fe oxides and $Ni(OH)_2$ concentrations were observed between the two passive regions.

4. Conclusion

The passive films formed on A600 and A800 were both bilayer oxides with a Cr rich barrier layer and a Ni/Fe rich outer layer. The segregation between these layers was much more prominent on A800 than on A600. A800 provided greater corrosion protection and retained the Cr barrier over a larger potential range than A600. For both alloys, the barrier layer was more protective than the outer layer. Higher concentrations of Cr_2O_3 in the barrier layer could be correlated to an increase in resistance. Changes in Ni and Fe hydroxide/oxide concentrations in the outer oxide resulted in little change in measured electrochemical impedance.

5. Acknowledgements

Funding from University Network of Excellence in Nuclear Engineering (UNENE) and Natural Sciences and Engineering Research Council (NSERC) is gratefully acknowledged.

6. References

[1] G. Sui, J. Titchmarsh, G. Heys, J. Congleton,*Corr. Sci.* **39** (1997) 565

[2] P.A. Page, A. McMinn, *Met. Trans*. **17A** (1986) 877

[3] M. Fontana. Corrosion engineering. McGraw-Hill, Inc. (1986)

[4] R.W. Staehle and J.A. Gorman, *Corrosion***59** (2003), p. 937 60 (2004) 5; 60 (2004) 115.

[5] R.W. Staehle and J.A. Gorman, *Corrosion***60** (2004), p. 5.

[6] R.W. Staehle and J.A. Gorman, *Corrosion***60** (2004), p. 115

[7] W. Zang, Z. Lu, D. Huang, D. Kong, G. Zhao, J. Congleton, *Corr. Sci*. **43** (2001) 963.

[8] M.G. Faichuk, S. Ramamurthy, W.M. Lau, Corr. Sci. **53** (2010) 1383.